Article

Mineralogical and Geochemical Evidence of Paragenetic Unity of Igneous Silicate and Carbonatite Rocks of the Tomtor Massif in the North-East of the Siberian Platform

Alexander Okrugin ![ORCID] and Anatolii Zhuravlev *![ORCID]

Diamond and Precious Metal Geology Institute, Siberian Branch of the Russian Academy of Science, 39, prosp. Lenina, Yakutsk 677000, Russia
* Correspondence: ai.zhuravlevgeo@gmail.com; Tel.: +7-4112-33-56-59

Abstract: The Tomtor massif is a polychronous ring zonal complex of alkaline ultramafic and carbonatite rocks containing unique Nb and REE deposits. Mineralogical and geochemical studies of minerals from different types of silicate rocks and carbonatites of the Tomtor massif were performed. For excluding traces of the interaction between silicate and carbonatite melts, we limited ourselves to the study of independent small secant bodies located in the immediate vicinity of the massif itself. The presence of through mineral series in various silicate igneous rocks and carbonatite ores of high-titanium chromium spinels, rare-metal, ore and other exotic phases with similar compositional trends was defined. Such studies will help reveal the mineralogical criteria for the genetic relationship between silicate melts and associated carbonatite derivatives, which can form rich rare elements mineralization. Also, such studies help to improve the petrochemical and mineralogical criteria for dividing potentially diamond-bearing magmatites (typical kimberlites) from non-diamond-bearing kimberlites, alpicrites and other non-diamond-bearing rocks convergent to kimberlites, which are formed under different physicochemical conditions. The existence of polychronous complex ore–magmatic ring complexes, such as the Tomtor massif, indicates the existence of large deep intraplate magma-generating chambers in the lithospheric mantle.

Keywords: alkaline–ultrabasic rocks; melteigite; alkaline picrite; syenite; carbonatite; rare earth elements; Tomtor massif

1. Introduction

The Tomtor massif, consisting of alkaline syenites, foidolites, picrites and carbonatites, contains a unique deposit of Sc-REE-Y-Nb ores. Geological structure and composition of the rocks of this massif were considered in the works of many researchers [1–8]. This 15 km × 20 km oval massif has a concentrically zonal structure and composed mainly of alkaline and nepheline syenites. The core of the massif consists of carbonatite rocks bordered by a rim of foidolites, i.e. nepheline-pyroxene rocks (Figure 1). Less common are dikes or tubular bodies of alkaline rocks with ultramafic composition, which various authors refer to as alnoites, alkaline picrites, lamprophyres, or lamproites. The age of the To-2 pipe defined by $^{40}Ar/^{39}Ar$ method on phlogopite is 379.4 ± 3 Ma [8], while the formation of the Tomtor massif itself and carbonatites mainly covered the Wendian-late Riphean and Middle Devonian time [2,9,10].

A weathering crust formed after all the rocks; the thickest crust formed after the carbonatites, which are enriched in phosphates and REE. The highest-grade ores contain on average 4.5% Nb_2O_5, 7%–10% REE_2O_3, 0.75% Y_2O_3, 0.06% Sc_2O_3 [11].
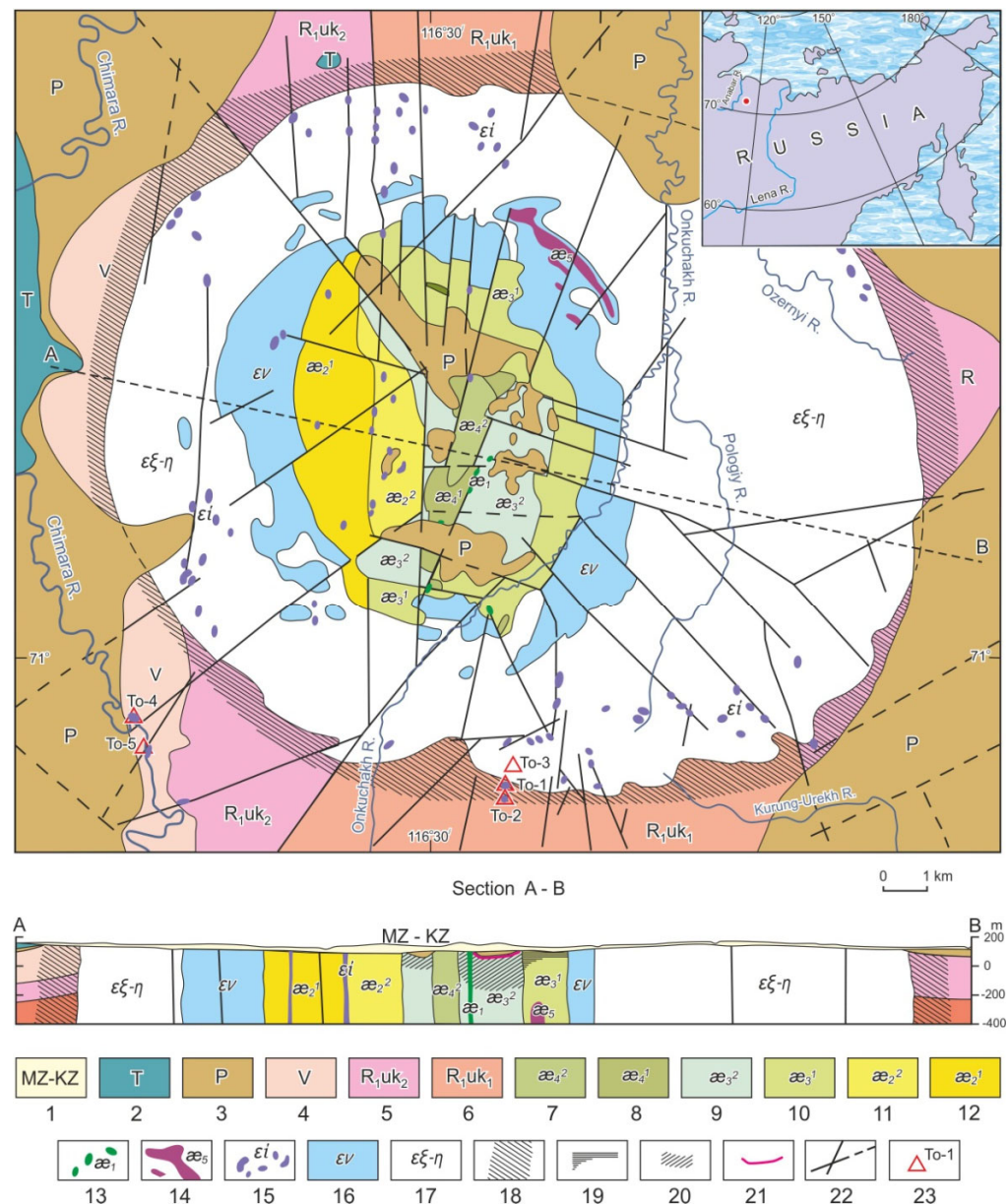
Figure 1. Schematic geological map of the Tomtor massif without Mesozoic–Cenozoic overlapping cover. Composed on geological base compiled by A.V. Tolstov [8] based on materials from a geological survey (1974–1983) and the results of the Ebelyakh GSP. In the inset, the Tomtor massif is marked with a red circle. 1—Mesozoic–Cenozoic silt-shales, sandstones, undivided gravelites (on section); 2—lower Triassic tuffs, lavas of plateau basalt; 3—Permian conglomerates, gravelites, sandstones, silt-shales, coals; 4—Vendian sandstones, gravelites, silt-shales; 5, 6—dolomites, shales, silt-shales, sandstones of Ulakhan–Kurug formation of Riphean: upper (5) and lower (6) suits; 7–14—carbonatite complex: 7—rare-metal carbonatites (ankerite), 8—ankerite–chamosite rocks, 9—rare-metal carbonatites (polymineral), 10—apatite–microcline–mica rocks, 11—hungry carbonatites (calcite and dolomite-calcite), 12—calcite–microcline–mica rocks, 13—carbonatite breccias, 14—kamaphorites (calcite–phlogopite–magnetite rocks); 15–17: silicate rocks complex: 15—small cross bodies of alkaline–ultrabasic rocks (alnoite, alkaline picrites, tinguaites and others), 16—foidolites (nepheline–pyroxene rocks of the jacupirangite–urtite series), 17—alkaline and nepheline syenites; 18–21—supergene complexes (on section): 18—marbling and skarning zones; 19—extended shape waste mantle; 20—deep waste mantle; 21—kaolinite–crandallite horizon, 22—tectonic deformations; 23—sampling sites with numbers of the sample.

Such ore-magmatic complexes can be sources not only of deposits of rare elements but also of precious metals, such as gold and platinum. This is confirmed by the wide distribution of areal complex gold platinum placers in the Anabar basin, where a silicate inclusion consisting of diopside, nepheline, phlogopite, titanomagnetite and amphibole was found in one grain of ferroan platinum [12,13]. Judging from the proportions of minerals and their microprobe compositions, the bulk composition of the inclusions (41.22 wt % SiO_2, 1.19 TiO_2, 15.14 Al_2O_3, 0.03 Cr_2O_3, 13.61 FeO_{tot}, 0.12 MnO, 9.71 MgO, 10.27 CaO, 5.02 Na_2O, 2.88 K_2O) corresponds to the rocks of the ijolite–melteigite series [14]. The results of preliminary studies of the petrochemical and mineralogical features of silicate igneous rocks and carbonatites of the Tomtor massif were presented in our abstract work [15]. This article is devoted to a more detailed consideration of the mineralogical characteristics of typical silicate igneous rocks (nepheline syenites, foidolites, alkaline picrites) and carbonatites of the Tomtor massif in order to identify convergent features among these petrotypically different, but paragenetically related rocks. The analysis of mineral associations of igneous rocks within the framework of experimentally studied phase diagrams of the "expanded basalt tetrahedron" Ne–Fo–SiO_2–La [16] allows us to interpret possible trends in the evolution of the Tomtor ore-magmatic system, as well as to draw some ore-genetic conclusions.

2. Materials and Methods

The classification of alkaline ultrabasic rocks, kimberlites and carbonatites of the north of the Siberian platform, as defined by their first researchers [17–20], continues to change [21–24]. Many variants for dividing such an association of geochemically and mineralogically related rocks are proposed: from the traditional distinguishing of two autonomous formations, alkaline–ultrabasic rocks, with carbonatites and kimberlites to their division into many formations according to different facies, material and other characteristics. Without discussing this complex problem, we still adhere to the point of view of [22,24] on the threefold division of the carbonatite–kimberlite formational rock assemblage into 1—diamond-bearing kimberlites; 2—kimberlite-like picrite–alnoite rocks (alpicrites) associated with rare metal carbonatites and 3—non-diamond-bearing and poor-diamond-bearing kimberlites, often called picrites or picrite porphyry ("kimpicrites") [18]. Such classification appeals to us because the use of the term "kimberlite" sensu stricto limits the use of this taxon to the area of diamond-bearing rocks containing diamond companion minerals, which is of great mineralogical prospecting and genetic significance.

As noted above, here we will try to show some convergent mineralogical features of silicate igneous rocks and carbonatite formations, which can serve as a criterion for assessing the genetic relationship between typical silicate magmas and carbonate igneous melt. However, the possibility of the existence of the latter, despite the direct facts of the outpouring of carbonate lava from volcanoes, is treated with distrust by some researchers, ranging from complete denial to a palliative (dual) version of the formation of carbonatites, for example, by the magmatogenic–metasomatic or hydrothermal–metasomatic ways.

In this regard, for the purity of the experiment, in order to exclude traces of the interaction of silicate and carbonatite melts, occurrence intensively in the central part of the massif, we limited ourselves to the study of independent small cross-cutting bodies located in the immediate vicinity of the massif itself (Figure 1). The studied tube bodies (To-1 and To-2) of melteigites intrude the Riphean sediments in the immediate vicinity (200–500 m) of the southern contact of the massif. A sample of fresh nepheline syenites was taken 0.5 km to the north of these bodies from the southern edge of the massif for study (To-3-1). A sheet body of alkaline picrites (To-4) was studied on the cliff of the right side of the Chimara river, 2 km southwest of the massif and not far from this body on the left side, a vertical dike-like transverse body (To-5) of carbonatites is partially outcropped.

The chemical compositions of minerals from the rocks of the Tomtor massif were determined on the "Cameca" Camebax-Micro microprobe analyzer (Gennevilliers, France), and their microstructural relationships were studied on the JEOL scanning microscope JSM-6480LV (Tokyo, Japan) in the laboratory of X-ray spectral analysis methods at DPMGI SB RAS, analyst—Khristoforova N.V. Standardized minerals, pure metals, and their alloys were used as standards. Chemical analysis of silicate rocks was performed in the Department of Physical and Chemical methods of Analysis at DPMGI SB RAS, supervisor—Galenchikova L.T. Due to the strong variability of some silicate rocks and carbonatites of the Tomtor massif, their X-ray phase analysis was performed on a diffractometer "Bruker" D2 PHASER (Billerica, MA, USA), CuKα emitting, 30 kV, 10 Ma, analysts—Yemelyanova N.N. and Tronina T.F. Identification of mineral phases was performed by Zayakina N.V. using the PDF 2 database.

3. Chemical and Mineralogical Features of Tomtor Massif Rocks

Compositions of the studied samples are shown in Table A1. There are no traces of altered secondary processes in the described bodies. This allowed us to determine some interesting convergent mineralogical features between silicate igneous and carbonatite rocks, indicating their deep genetic relationship. Many variants of diagrams of the component composition of alkaline ultramafic rocks, kimberlites, and carbonatites, were considered. We propose the following M–S–C–H_2O diagram for a comparative analysis of these rocks (Figure 2). Its ternary system is constructed in coordinates: M—femic (mafic) components ($MgO + FeO_{tot} + MnO + TiO_2 + P_2O_5$); S—alkaline–sialic components ($SiO_2 + Al_2O_3 + Na_2O + K_2O$) and C—volatile components ($CO_2 + H_2O$) and CaO. It resembles the Holmes diagram [25], but we moved the CaO from the cafemic top to the volatile components in order to better distinguish the carbonatite trend (C) from the mafic (M) and alkaline–sialic (A).

The lower double system ($CaO + CO_2 + H_2O$)–H_2O shows the role of water in the composition of volatiles. With the CaO increase in carbonatites, the water content gradually decreases, and closer to the top (C), its amount is practically reduced to zero, i.e., in essentially calcite carbonatites, the role of water is negligible. With an increasing proportion of other petrogenic oxides in intrusive carbonatites, the water content gradually increases, and the fields of carbonatite compositions are adjoining to kimberlites. Increased water content is typical for kimberlites and meimechite, usually 4–10 wt.%, rarely reaching 13–14 wt.%. This is expressed in the wide spreading of water minerals in these rocks, in particular, the serpentinization of olivine. In the carbonatite breccias of the Eastern Anabar region [21], alkaline basaltoids [26], melilite rocks [20], and olivinites from the ring massifs [27] of the Maymecha–Kotuy province, as well as in the syenites of the Tomtor massif, the water content rarely exceeds 4%.

We assume [8] that the parent melt of the Tomtor massif was close to the picrite porphyrites of the Guli massif, and fractional cristallization during the precipitation of olivine and chromespinelide according to [27] leads to the appearance of meimechites, and then dunites (Figure 2, trend M). This original composition of the Tomtor massif parent melt corresponds to alkaline picrites To-4 and melteigites To-(1, 2). Nepheline syenites To-3 are, apparently, alkaline–sialic differentiates (trend A). Figure 2 shows that the Tomtor massif rocks form a second well-distinct carbonatite trend (C) as a result of CaO and CO_2 progressively increasing in them. To-5 rocks are a transitional variety from ordinary silicate magmatites to typical carbonatites, which usually contain more than 50 wt. % carbonate and less than 10%–15% silica.
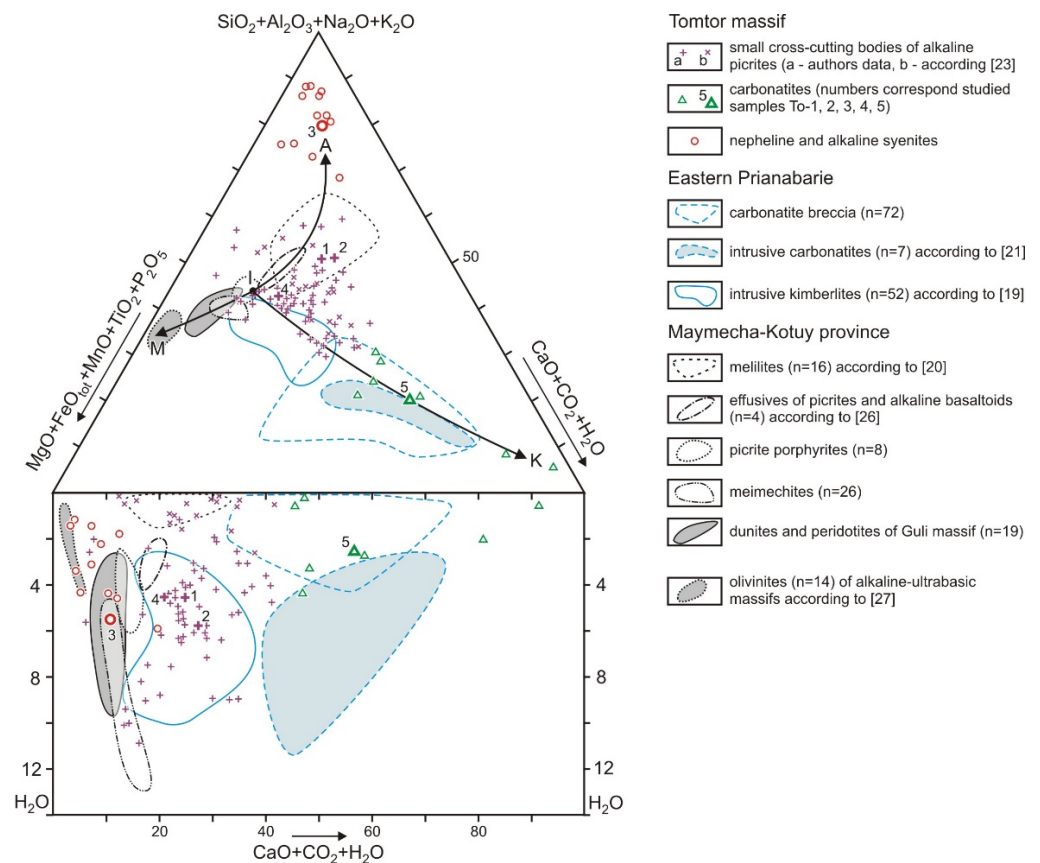
Figure 2. Compositions of rocks from alkaline, ultrabasic, kimberlite and carbonatite complexes (n—amount of analysis) in the north of the Siberian platform on the M–S–C–H_2O diagram (wt. %). Curved lines with arrows—trends of changes of initial composition of picrite magma (I) to ultramafic (M), alkaline–sialic (A) and carbonatite (K) differentiates.

The essential minerals of the melteigites of the To-1 and To-2 pipe bodies are pyroxene of diopside–augite composition ($Wo_{35-50}En_{24-41}Fs_{9-25}$), less often, aegirine–augite and mica of the phlogopite–biotite series (Table A2). They form porphyry particles in the fine-grained calcite–natrolite–mesolite groundmass with abundant inclusions of apatite, tita–omagnetite in association with leucoxene, titanite, perovskite, and andradite–schorlomite garnet (Figure 3A–C). The smallest inclusions of carbonates of rare earth elements (REE), calkinsite, ambathorianite and carbocerianite, are less common. Some grains of REE carbonates contain up to 20% WO_3, which indicates a high proportion of Ce–tungstite minal ($(Ce,Nd,Y)W_2O_6(OH)_3$. The most representative mineral analysis is presented in Tables A2 and A3, and their figurative points are placed on the composition diagrams (Figures 4–6). Natrolite–mesolite zeolites are typical products of nepheline alteration, i.e., according to their chemical composition and mineral associations, these rocks belong to alkaline (plagioclase-free) rocks undersaturated in silica, corresponding to melteigites.
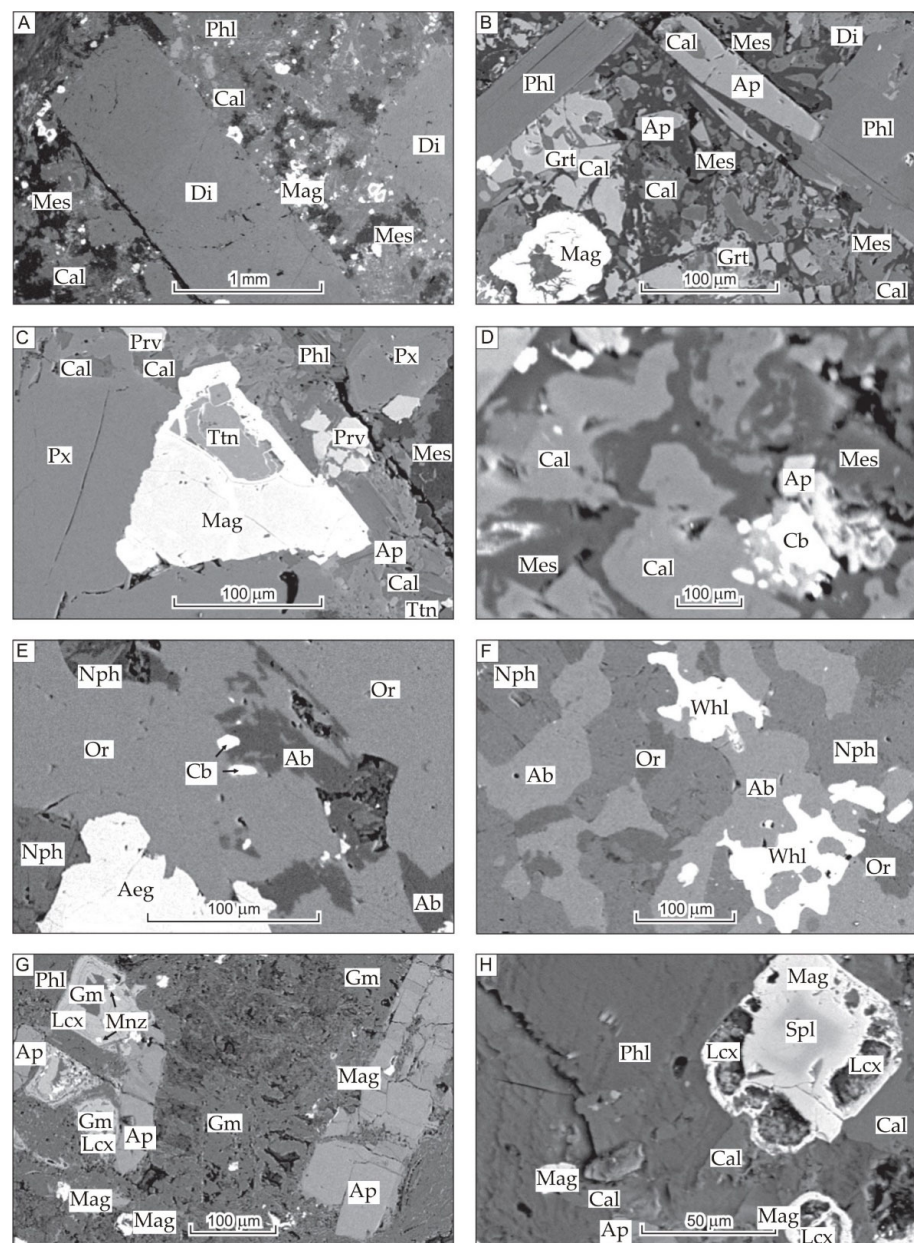
Figure 3. Rock-forming and ore minerals from rocks of Tomtor massif. (**A–D**)—melteigites (samp. To-1-2): (**A**)—porphyry of diopside (Di) in the groundmass of phlogopite (Phl), calcite (Cal), mesolite (Mes) and magnetite (Mag); (**B**)—porphyry crystals of phlogopite (Phl) in grained groundmass that contained diopside (Di), calcite (Cal), mesolite (Mes), magnetite (Mag), garnet (Grt) and apatite (Ap); (**C**)—intergrowth of pyroxene (Px), magnetite (Mag), titanite (Ttn) and perovskite (Prv), surrounded by phlogopite (Phl)–calcite (Cal)–mesolite (Mes) groundmass; (**D**)—small particles of REE carbonates (Cb) in association with apatite (Ap) in calcite (Cal)–mesolite (Mes) symplectite mass: (**E,F**)—nepheline syenites (samp. To-3-1): (**E**)—small inclusions of REE carbonates (Cb) in albite (Ab)–orthoclase (Or) micro perthite in concrescence with nepheline (Nph) and aegirine (Aeg); (**F**)—"amoeba-shaped" inclusions of wohlerite (Whl) in nepheline (Nph)–albite (Ab)–orthoclase (Or) symplectite matrix; (**G,H**)—carbonatites (samp. To-5-1): (**G**)—euhedral crystals of apatites (Ap) and "case-shaped" zoned substance of leucoxene (Lcx) with small inclusions Ce–monazite (Mnz) in clay–siderite–calcite (Gm) groundmass; (**H**)—zoned grain magnetite (Mag) with a relict core of chromium spinellid (Spl) in intergrowth with phlogopite (Phl) and calcite (Cal). Image in back-scattered electrons.

In regard significant late magmatic auto-metasomatic alterations of rocks and small sizes of inclusions of accessory and ore phases, in this article, we used a limited range of representative microprobe analysis, confirmed by X-ray phase analysis on a diffractometer. On the classification diagrams, pyroxenes from melteigites mainly fall into the fields of diopside and augite, less often aegirine–augite or aegirine (Figure 4), and micas are located mainly in the phlogopite region, partially passing into the annite field (Figure 5A). Garnet compositions vary from almost pure andradite to a field of melanites of Ti–andradite (Figure 5B), covering a wider area than the garnets we found in kamaphorites of the Tomtor massif [28].
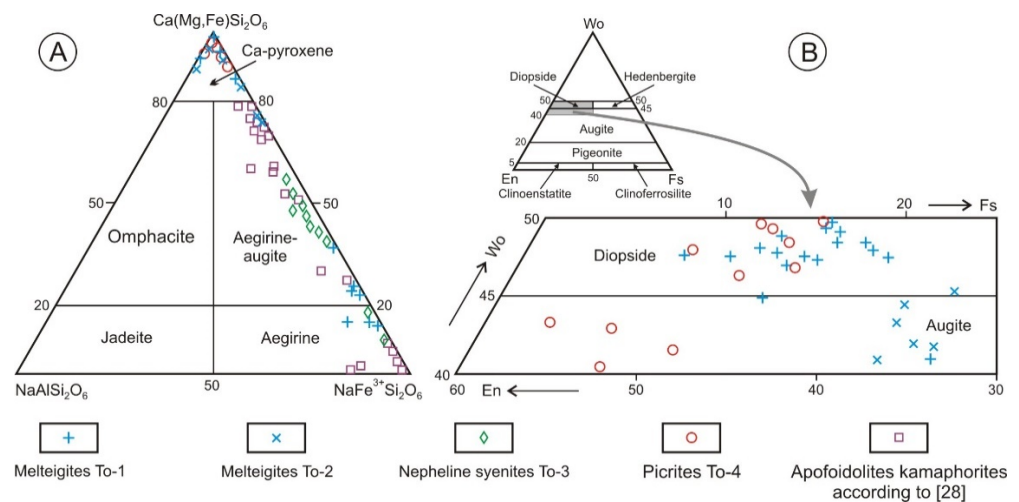
Figure 4. Composition of pyroxenes on Ca–Mg–Fe–pyroxenes–jadeite–aegirine (**A**) and En–Wo–Fs (**B**) diagrams.

The rocks of the sheet-like body To-4 differ from the melteigite bodies considered above by a higher magnesian content but a lower content of aluminum, calcium and sodium (Table A1), which is reflected in their mineral composition. Pyroxene is characterized by an increased proportion of enstatite minal ($Wo_{40–50}En_{35–46}Fs_{5–13}$) and phlogopite. In general, it has a more magnesian composition and a serpentinized olivine appearance. The carbonate in them is represented by dolomite, mesolite typical for melteigites is replaced by less calcic natrolite. Along with chromium (Cr_2O_3 up to 20%) titanomagnetites (5%–13% TiO_2), there are also significantly titanium-bearing (0.5%–7.5% TiO_2) chromespinelids (Cr_2O_3 20%–46%). All these chemical and mineral features bring these rocks closer to the picrites of alkaline grade and meimechites.

In syenites To-3-1, along with nepheline (Figure 3E,F), orthoclase with microperthite ingrowths of albite and hyalophane containing up to 10%–20% BaO were widely spread, which corresponds with a celsian composition of around 20%–30%. Pyroxene is represented by aegirine, and rare small mica particles are represented by muscovite. Small (up to 10–20 microns) inclusions of REE carbonate, similar in composition to calkinsite, are observed in the fresh nepheline-K-Na-FS groundmass of syenites. Moreover, larger (up to 150 microns) amoeba-shaped interstitial particles of wohlerite consisting of 30%–32% SiO_2, 1-3.5 TiO_2, 25-27 CaO, 7-8 Na_2O, 14-17 ZrO_2 and 12-16 Nb_2O_5 were found. Wohlerite is an accessory mineral of nepheline syenites and is related to pegmatites and carbonatites.

Small inclusions of REE carbonates were also found in melteigites (To-1 and To-2); their composition is similar to minerals from kamaphorites of the Tomtor massif [28]. In some grains of REE carbonates from the To-1-2 sample, a high content of WO_3 up to 20% is defined (Table A3); apparently, these phases contain a large proportion of Ce–tungstite minal, the mineral $(Ce,Nd,Y)W_2O_6(OH)_3$ found in cassiterite–wolframite ores occurring on tourmaline granites of Malaysia.
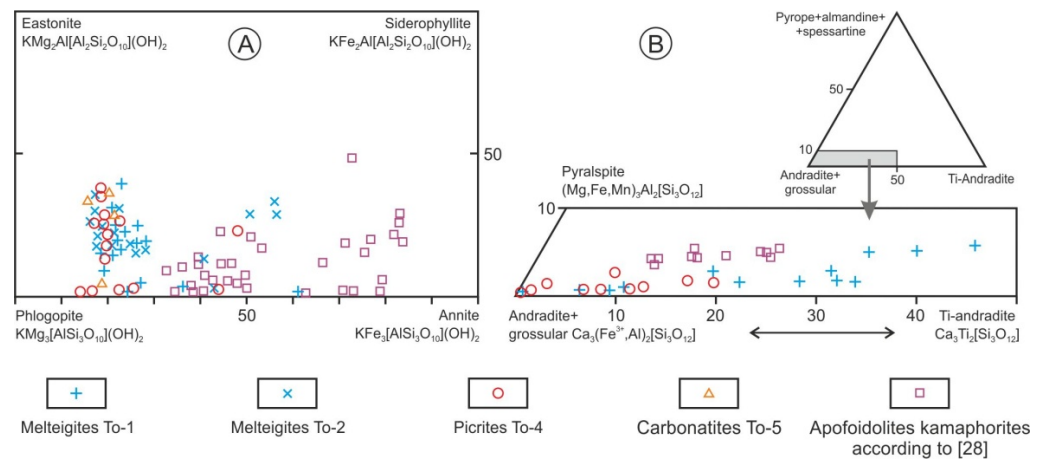
Figure 5. Composition diagrams of biotites (**A**) and garnets (**B**).

Apatite in the melteigites of the pipe bodies To-1 and To-2 occurs mainly in the form of idiomorphic elongated crystals of the hexagonal cross-section in the groundmass of the rock, usually closely associated with ore–oxide ilmenite–titanomagnetite aggregates, as well as small (1–50 microns) sulfide minerals, such as pyrite and galena. The composition of the mineral corresponds to the fluorine-containing (F up to 2%–2.4%) variety of apatite. In some analyses, according to micro-probe analysis, the P_2O_5 content is reduced to 35%–38% instead of the usual 40%–42%, which is probably due to an increase in the amount of CO_2 and the appearance of carbonate–apatite or francolite in the presence of F > 1%. In such cases, due to the impossibility of determining the CO_2 content with the micro-probe, the amount of analyses of carbonate apatites steadily decreases to 90%–88%. They also show the frequent occurrence of minor (no more than a few %) impurities of other petrogenic elements, which is probably caused by the capture of micro inclusions of the silicate matrix. The role of carbon in the carbonate–apatite structure has not yet been fully resolved, but we are inclined to associate the decrease in the proportion of P_2O_5 in To-1-2 francolites with the $PO_4 \leftrightarrow CO_2$ isomorphism rather than the substitution of the CO_3 group for the (OH, F, Cl) or C $\leftrightarrow$ 2Ca group. In the picrites of the sheet-like body To-4 and the carbonatite of dike To-5, all apatites have a low P_2O_5 content of 34%–39% with a low total (less than 90%–93%) of analysis, which also indicates their belonging to carbonate–apatites.
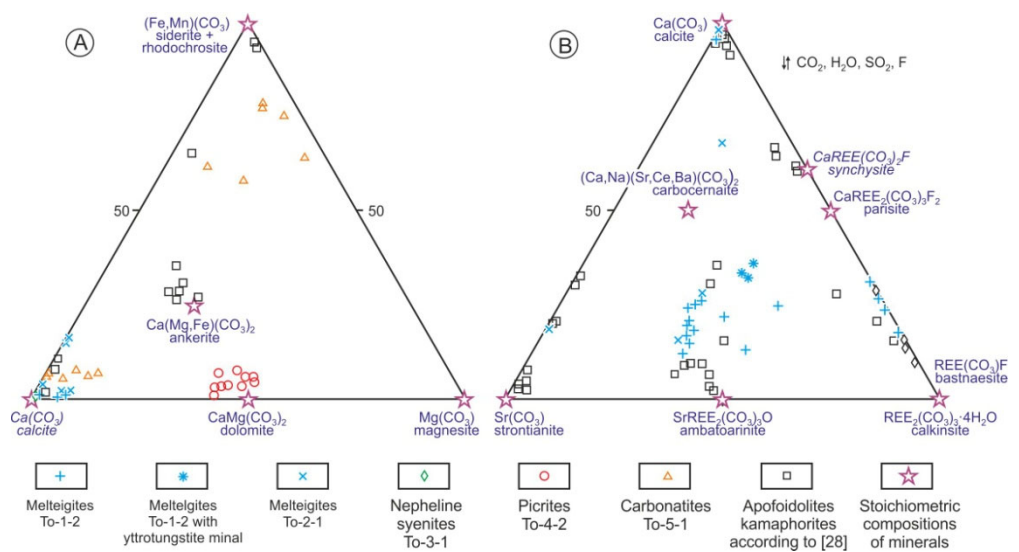

Figure 6. Compositions of main carbonate minerals (**A**) and rare carbonates of Sr and REE (**B**).

An interesting general characteristic feature of alkaline picrites To-4 and carbonatites To-5 is the similarity of trends of change in chromium–titanium spinels (Figure 7), similar to those of alkaline–ultrabasic rocks of the Guli massif [29], picrite gabbro–dolerites of the Norilsk region [30,31], poor diamond-bearing kimberlite the Malokuonamskaya pipe [32] and other high-Ti alkaline picrite rocks of the Anabar region [12]. In the relic cores of Ti–Cr-spinels in To-5 carbonatite, the content of Cr_2O_3 reaches 43% (Figure 3H, Table A4), and towards the grain periphery, with a decrease in spinel chromium content, its titanium content increases. Ti-magnetites To-5 contain a constant admixture of MnO 1%–2% and MgO up to 5%. In melteigites To-1 and To-2, titanomagnetites have a similar composition, but in association with magnetite, small grains of Mn–ilmenite containing MnO from 2 to 22% appear in them.

Carbonatite of the To-5 dike mainly consists of calcite with an increased admixture of FeO and MgO up to 4% of each oxide. Perhaps this explains the wide spread of siderite, containing up to 13% CaO, 11% MgO, and 4% MnO, in the form of thin (up to 50 μm) network veinlets, in the calcite matrix. Calcite is also closely intergrown with chlorite and montmorillonite (Table A2), among which sheath-like zonal segregations of leucoxene with a calcite core are often found (Figure 3G). The smallest xenomorphic light inclusions enriched in TiO_2 up to ~40%, Ce_2O_3 up to ~20% and P_2O_5 up to ~10% are often observed within the leucoxene shell. If we assume that the microprobe beam partially captures the leucoxene matrix due to the small size of the bright-colored inclusions, then the true composition of the inclusions themselves can correspond to Ce–monazite. Thus, we consider that these studies are preliminary and require their continuation on more extensive material.
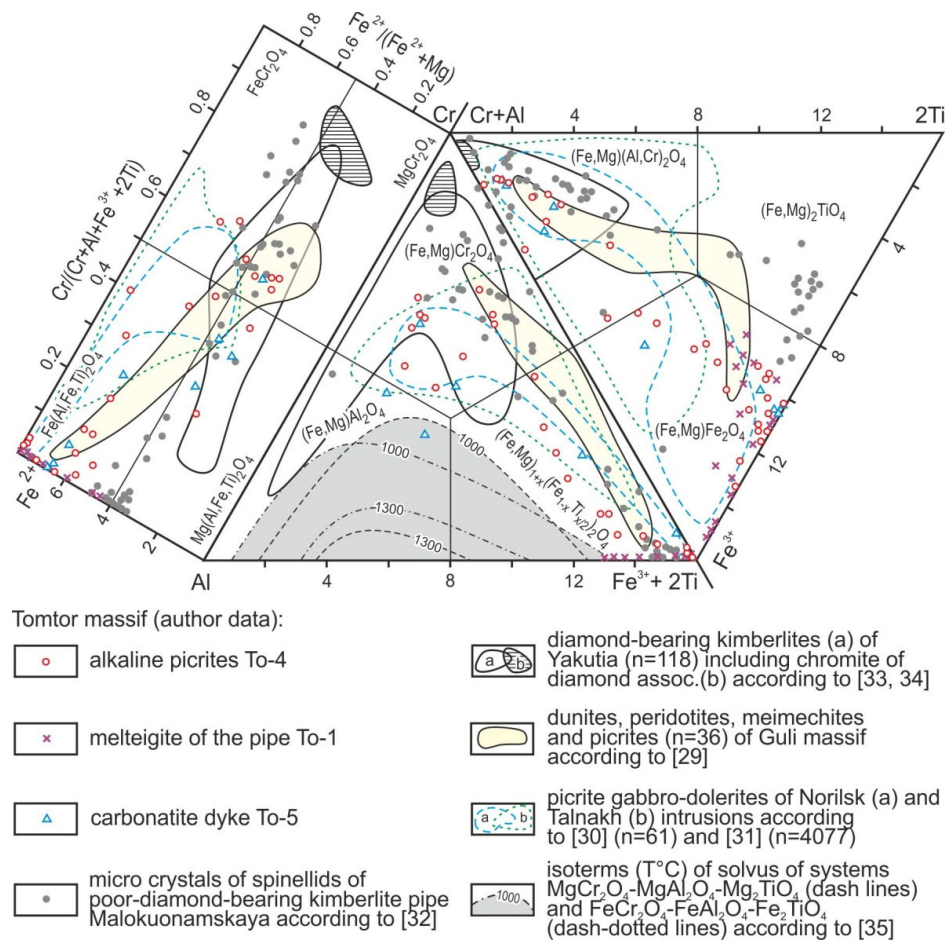
Figure 7. Composition of spinellids (n—number of analyses) from rocks north of Siberian platform [29,31–35].

4. Discussion

As we previously showed [8], even slight changes in the SiO_2 and CaO content of alkaline magmas can radically change the crystallization trends of the original picritoid magma. The diagram (Figure 2) shows the following trends leading to the formation of different rock associations in the process of a long evolutionary formation of complex alkaline–ultrabasic complexes from the initial alkaline picrite melt. Early high-temperature intensive crystallization and jigging of olivine with chrome spinel leads to the forming of accumulative rocks–dunites, as in the Guli massif. "Dry" olivinites from the smaller massifs of the Maymecha–Kotuy province are characterized by a very fresh appearance, olivine in them is almost not serpentinized and is associated with magnetite [27]. The magnesian trend leads the compositions of these rocks away from the initial composition of picrites towards the M-top of the diagram: peridotite–dunites and olivinites. Another compositional change trend, as a result of the accumulation of alkalis and CaO, is traced towards almost anhydrous melilite rocks through an intermediate field of effusive alkaline basaltoids. Further, there is a separate field of alkaline and nepheline syenites, which are predominantly distributed in the Tomtor massif.

The existence of the above-mentioned two trends can be explained in terms of experimental data on the phase relations of the expanded alkaline–basalt tetrahedron Ne–Fo–SiO_2–La(Ca_2SiO_4) [16]. The assumed initial melt of alkaline ultrabasic complexes has an olivine–diopside–nepheline composition, i.e., accordingly, it is located not far from the Ne–Fo–Di section of the alkaline–basalt tetrahedron, where a temperature maximum was experimentally established on the Ne–Fo–Di–L cotectic line separating the invariant points Ne–Mel–Fo–Di and Ne–Pl–Fo–Di. Thus, even small variations in the CaO content in the initial melt, for example, as a result of long-term differentiation of magma in deep intermediate chambers or contamination by host carbonate rocks, can lead to melilite or nepheline trends in rock composition changes. Changing trends in the composition of such melts during fractional crystallization can be traced in the triple diagrams of phase equilibria shown in Figure 8. In the diopside–forsterite–silica system, a temperature maximum is established, which is located near (slightly to the left) the point of intersection of the Fo_{ss}–Di_{ss} boundary curve with the Di–En conoid (point "C" in Figure 8).

Thus, the plane passing through the diopside solid solution, the maximum point (C), and the forsterite solid solution is a new temperature barrier separating olivine–tholeiite magma from alkaline basaltic magma [36]. Consequently, the crystallization of the melt of composition E, located in the Fo–Di–C field, will start from the enstatite-containing composition and proceed along the Fo–Di cotectic to the triple akermanite-bearing Fo–Di–Ak eutectic, crossing the Fo–Di line, which is pseudo-binary. This is due to the fact that forsterite and diopside can contain monticellite and enstatite molecules, respectively, forming solid solutions. As microprobe analyses show, olivines from alkaline–ultramafic rocks have an increased content of CaO, sometimes reaching 2.8 wt.% (~8 mol.% monticellite), which we found in the rocks of the Kugda massif. If the composition of the initial melt also shifts towards SiO_2 enrichment (point "D" in Figure 8), then the course of crystallization will change into the opposite trend of saturation of the residual melt with silica.

Such a course of trends in boundary composition changes can be observed in the triple diagrams containing the Na-component of nepheline (Figure 8B,C). Shown here are the trends in the compositions F and G that are close to each other. Trends in the compositions F and G that are close to each other are shown in the plot. However, as can be seen from the adjacent diagrams, even a slight deviation in the content of silica can cause a change in the composition of rocks from melilite-bearing to quartz-normative differences.
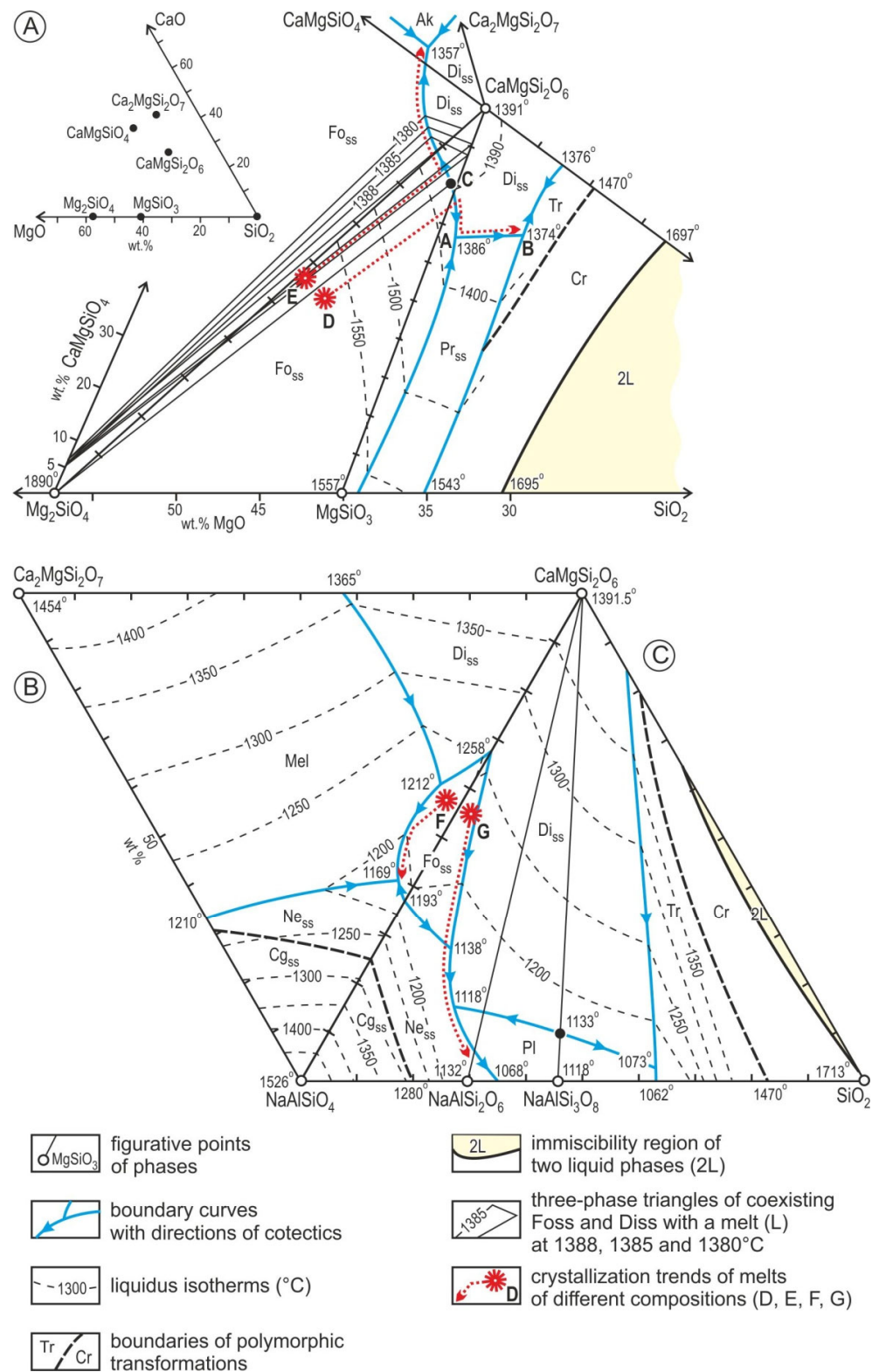
Figure 8. Possible crystallization trends of various rock associations of the Tomtor massif on multidiagrams of Fo–Ak–Di–Ne–Q. Diagrams: Fo–Di–SiO$_2$ (**A**) according to [36], Ne–Ak–Di (**B**) according to [37], Ne–Di–SiO$_2$ (**C**) [38]. The inset shows the positions of main minerals in the MgO–CaO–SiO$_2$ system. Fields of crystallization of phases: Fo—forsterite; Di—diopside; Pr—protoenstatite; Ak—akermanite; Cg—carnegieite; Ne—nepheline; Pl- plagioclase; Mel—melilite; Ab—albite; Cr—cristobalite and Tr—tridymite. Other explanations in the main text.

The genetic unity of the complexes of ultrabasic, alkaline rocks and carbonatites is confirmed not only by the structural connection but also by the similarity of petrochemical and mineralogical features. Many researchers adhere to the model of partial melting of magmas with a rich rare-metal specialization from a metasomatically enriched mantle. According to V.S. Shkodzinsky [39], alkaline–ultrabasic, kimberlite, carbonatite and lamproite magmas are residual melts arising from the fractional solidification of the lower picrite and peridotite layers of the global magmatic ocean of the Earth.

The most acute problem in the genesis of complexes of alkaline–ultrabasic rocks with carbonatites is to elucidate the nature of the interaction between carbonatite and silicate melts. The almost ubiquitous close spatial and temporal connection of carbonatite massifs with complexes of alkaline ultrabasic rocks and syenites allowed A. Hegbom, W. Bregger, R. Delhi and G. Eckerman to put forward a position on the igneous origin of carbonatite formations. Based on experimental data on many carbonate-bearing systems [40], P. Willey concluded that there is an immiscibility of silicate and carbonate magmas, which determines the possibility of separating carbonatite melts and fluids from the parent alkaline–peridotite magma. As a real of the existence of immiscibility between silicate and carbonatite magmatic melts, various researchers cite numerous facts [41,42] about the existence of alkaline rocks of globules and melt inclusions of carbonate composition in minerals, including deep ones. The fact of separation of the calcite phase from the silicate melt at the magmatic stage by segregation was described in the example of a differentiated sill of analcime basaltoids in Kazakhstan [43]. In the middle part of the sill, accumulations of small (up to 5 mm) spherical calcite globules are observed, which, when merging up the section, become larger and acquire complex shapes, forming individual nests up to 10–20 cm in size, lenticular segregations and veinlets of calcite.

As a result of the study of silicate–salt inclusions in minerals, L.I. Panina and I.V. Motorina [44] prove the silicate-carbonate immiscibility is the reason for the appearance of the initial carbonatite melts associated with deep-seated magmas. It is also interesting to note that the fact of melt separation into two immiscible liquid phases with a sharp boundary was established as a result of direct experimental–technological melting of pyrochlore–monazite and pyrochlore–monazite–crandallite samples from the Tomtor massif itself [45].

5. Conclusions

New data indicating the convergent features of rock-forming, secondary, accessory and ore minerals of silicate igneous rocks of the Tomtor massif and associated carbonatite formations were obtained as a result of mineralogical and geochemical studies. The presence of through mineral series in various silicate igneous rocks and carbonatite ores of high-titanium chromium spinels, rare-metal and other ore phases with similar compositional trends was established. The absence of grossular–almandine–pyrope minerals, diamond association chromites, picroilmenites and other high-pressure indicator phases characteristic of diamond-bearing kimberlites and lamproites indicates lower P-T parameters of the deep evolution of the Tomtor parent magma. In a time of multiple tectonic and magmatic movements in the north of the Siberian platform, a unique combination of alkaline–ultrabasic, kimberlite, carbonatite, high-titanium alkaline and tholeiite mafic rocks of different ages has formed. They are formed in the lithosphere and, therefore, form complex complexes of different ages that are spatially united, similar to the Tomtor massif. The predominant gravitation of complexes alkaline–ultrabasic rocks to the periphery of the Siberian platform can be associated with the formation of large igneous provinces (L.I.P.) as a result of the splitting of the Rodinia supercontinent, which began in the Neoproterozoic [46]. Depending on the physicochemical parameters of melting, the degree of differentiation, contamination, and other factors, complex ore-magmatic complexes can form, which are sometimes renewed during subsequent stages associated with a changing geodynamic situation of the region.

Appendix A

Table A1. Compositions of studied samples from rocks of Tomtor massif (all values in %).

Sample	SiO$_2$	TiO$_2$	Al$_2$O$_3$	Fe$_2$O$_3$	FeO	MnO	MgO	CaO	Na$_2$O	K$_2$O	P$_2$O$_5$	H$_2$O$^+$	CO$_2$	p.p.p.	Total
To-1-2	33.72	3.23	11.36	7.86	3.37	0.23	7.44	16.75	3.40	2.33	0.89	4.54	3.76	0.69	99.57
To-2-1	31.70	2.73	11.79	5.19	4.83	0.32	5.75	15.65	4.84	2.91	1.26	5.71	5.95	0.46	99.09
To-3-1	49.50	0.76	19.37	4.74	1.41	0.21	1.47	3.07	7.42	3.48	0.06	5.50	2.33	0.18	99.50
To-4-2	31.25	2.87	8.38	10.29	5.82	0.18	15.18	11.12	0.63	2.57	1.22	4.45	5.37	0.65	99.98
To-5-1	14.12	1.86	5.17	6.71	7.18	0.34	4.99	29.23	0.21	0.82	1.25	2.60	24.96	0.50	99.94

Table A2. Representative analyses of silicate minerals (all values in %; nd—not detected).

Sample	Analysis	SiO$_2$	TiO$_2$	Al$_2$O$_3$	Fe$_2$O$_3$ *	FeO	MnO	MgO	CaO	Na$_2$O	K$_2$O	Total
				Diopside (12-183; 283), augite (23-2; 20-10; 287), aegirine (11-27; 4-7)								
To-1-2	12-183	44.93	2.74	6.57	1.23	6.09	0.09	13.02	24.43	0.48	nd	99.58
To-1-2	23-2	46.78	2.64	2.66	4.70	13.11	0.10	8.51	20.18	1.82	nd	100.50
To-1-2	11-27	49.91	1.72	1.66	30.08	0.00	0.08	1.76	2.71	12.41	nd	100.32
To-2-1	20-10	49.59	1.76	2.05	nd	15.83	0.52	9.58	21.09	0.10	nd	100.52
To-4-2	283	51.74	0.89	0.65	2.31	6.01	0.30	12.76	24.09	0.90	nd	99.64
To-4-2	287	50.49	1.62	2.65	2.59	5.43	0.21	13.79	20.62	1.22	nd	98.63
To-3-1	4-7	51.41	0.23	0.40	17.70	8.75	0.12	2.21	12.65	6.86	nd	100.33
				Phlogopite (11-5; 3-7; 23-10), annite (11-11; 18-183), muscovite (20-3)								
To-1-2	11-5	39.34	nd	11.40	1.61F **	12.28	nd	20.16	nd	nd	10.44	95.22
To-1-2	11-11	37.73	nd	11.04	nd	28.38	nd	9.95	nd	nd	9.80	96.90
To-4-2	3-7	37.13	6.32	15.12	nd	8.52	nd	19.80	nd	nd	9.18	96.07
To-4-2	18-183	40.80	0.93	11.03	nd	20.25	0.35	12.21	0.54	0.34	8.86	95.30
To-5-1	23-10	37.25	5.08	16.72	nd	9.78	nd	19.59	nd	nd	8.98	97.40
To-3-1	20-3	45.90	nd	36.02	nd	nd	nd	nd	nd	3.89	7.30	93.11
				Mesolite (14-1), natrolite (23-5; 7-1), chlorite (26-1), montmorillonite (19-2)								
To-1-2	14-1	41.65	nd	31.19	nd	nd	nd	nd	5.19	11.31	nd	89.33
To-1-2	23-5	46.62	nd	27.78	nd	nd	nd	nd	1.95	14.71	nd	91.06
To-4-2	7-1	47.52	nd	27.34	nd	nd	nd	nd	0.32	16.42	nd	91.60
To-5-1	26-1	33.91	nd	15.61	nd	13.42	nd	22.59	nd	nd	1.63	87.16
To-5-1	19-2	54.69	nd	18.12	nd	9.76	nd	3.62	1.55	nd	0.88	88.62
				Nepheline (19-1), orthoclase (5-5), albite (5-7), hyalophane (5-12; 16-4)								
To-3-1	19-1	43.29	nd	32.84	nd	nd	nd	nd	nd	15.54	5.97	97.64
To-3-1	5-5	64.25	nd	19.81	nd	nd	nd	nd	nd	1.29	14.75	100.10
To-3-1	5-7	68.51	nd	20.20	nd	nd	nd	nd	nd	11.67	0.28	100.66
To-3-1	5-12	47.31	nd	30.73	10.95BaO **	nd	nd	nd	nd	1.18	7.52	1.08	98.77
To-3-1	16-4	43.81	nd	28.27	19.84BaO **	nd	nd	nd	nd	4.05	2.20	98.17
				Andradite (14-5; 5-10), schorlomite (14-12; 10-8)								
To-1-2	14-5	34.86	3.24	2.23	26.21	nd	nd	nd	34.37	nd	nd	100.91
To-1-2	14-12	33.36	12.56	2.21	18.29	nd	nd	nd	33.17	nd	nd	99.59
To-4-2	5-10	34.16	2.95	14.01	12.17	nd	nd	1.84	35.01	nd	nd	100.14
To-4-2	10-8	34.29	6.20	nd	26.01	nd	nd	nd	33.50	nd	nd	100.00

*—Fe$_2$O$_3$ content calculated according to stoichiometric mineral formula; **—another element content showed, defined in this mineral (F and BaO).

Table A3. Composition of REE carbonates (all values in %; nd—not detected).

Sample	Analysis	CaO	SrO	WO$_3$	Ce$_2$O$_3$	La$_2$O$_3$	Nd$_2$O$_3$	Total	Mineral
To-1-2	29-2	3.66	nd	nd	29.17	20.25	7.84	60.92	Calkinsite
To-1-2	20-2	6.43	11.75	nd	20.84	12.62	4.70	56.34	Ambatoarinite
To-1-2	27-2	5.62	18.01	nd	21.51	12.36	7.61	65.11	Ambatoarinite
To-1-2	22-6	5.60	nd	20.00	20.90	10.96	5.47	62.93	La-Ce-tungstite
To-1-2	23-8	6.44	nd	18.70	22.31	13.80	5.38	66.63	La-Ce-tungstite
To-2-1	2-2	20.32	9.06	nd	19.25	8.71	nd	57.34	Carbocerianite
To-2-1	3-4	6.17	16.79	nd	27.84	13.31	nd	64.11	Ambatoarinite
To-2-1	20-7	3.17	19.57	nd	19.01	10.21	8.79	60.75	Ambatoarinite
To-3-1	3-7	1.59	nd	nd	31.22	22.37	nd	55.18	Calkinsite
To-3-1	15-3	1.78	nd	nd	31.33	17.96	6.96	58.03	Calkinsite
To-3-1	15-7	3.26	nd	nd	28.78	13.86	5.69	51.59	Calkinsite

Table A4. Representative analyses of Cr–Ti-spinels and magnetites (all values in %).

Sample	Analysis	TiO$_2$	Al$_2$O$_3$	Cr$_2$O$_3$	Fe$_2$O$_3$	FeO	MnO	MgO	Total
To-4-l	9-116	3.54	6.03	45.76	11.58	24.86	0.40	6.86	99.03
To-4-l	3-116	3.58	6.20	42.14	16.17	21.18	0.48	9.18	98.93
To-4-l	16-116	0.55	11.71	35.46	21.47	20.00	0.36	8.60	98.15
To-4-l	18-116	7.45	5.36	30.58	19.67	28.31	0.49	6.58	98.44
To 4-1	22-116	6.89	7.79	18.64	33.13	18.86	0.48	12.51	98.30
To-4-1	285-183	9.19	6.36	7.56	36.86	31.97	0.94	4.66	97.54
To-4-1	283-183	7.35	0.22	1.31	54.10	28.61	0.80	5.03	97.42
To-5-1	9-179	2.12	14.68	43.26	9.00	16.97	0.44	11.94	98.41
To-5-1	20-1	2.28	23.67	31.91	10.71	16.25	0.32	13.74	98.88
To-5-1	23-4	5.31	21.72	23.84	14.68	21.62	0.55	11.88	99.60
To-5-1	4-5	5.38	5.01	17.12	36.14	29.85	1.12	4.35	98.97
To-5-1	20-9	12.03	0.37	1.11	45.80	35.92	1.55	2.99	99.77

References

1. Epshtein, E.M.; Anikeeva, L.I. Some Issues of Geology and Petrology of the Complex of Ultrabasic Alkaline Intrusive Rocks. *Phys. Chem. Probl. Form. Rocks Ores. V* **1963**, *2*, 182–195. (In Russian)
2. Entin, A.R.; Zaitsev, A.I.; Nenashev, N.I.; Vasilenko, V.B.; Orlov, A.I.; Tyan, O.A.; Ol'khovick, Y.A.; Ol'shtinky, S.I.; Tolstov, A.V. On the Sequence of Geological Events Associated with the Intrusion of the Tomtor Massif of Ultramafic Alkaline Rocks and Carbonatites (North-Western Yakutia). *Geol. Geophys.* **1990**, *31*, 42–51. (In Russian)
3. Kravchenko, S.M.; Pokrovskii, B.G. The Tomtor Alkaline Ultrasbasic Massif and Related REE-Nb Deposits. Northern Siberia. *Econ. Geol.* **1995**, *71*, 676–689. [CrossRef]
4. Tolstov, A.V. Mineralogical and Geochemical Features of Apatite-Magnetite Ores of Tomtor Massif (North-Western Yakutia). *Geol. Geophys.* **1994**, *35*, 91–100. (In Russian)
5. Tolstov, A.V.; Tyan, O.A. *Gology and Ore Potential of Tomtor Massif*; YSC SB RAS: Yakutsk, Russia, 1999. (In Russian)
6. Bagdasarov, Y.A. Geochemical Features of Carbonatites and Related Silicate Rocks of Alkaline-Carbonatite Tomtor Massif (Eastern Prianabarye. Yakutia). *Geochemistry* **1997**, *35*, 10–20. (In Russian)
7. Panina, L.I.; Rokosova, E.Y.; Isakova, A.T.; Tolstov, A.V. Mineral composition of alkaline lamprophyres of the Tomtor massif as reflection of their genesis. *Russ. Geol. Geophys.* **2017**, *58*, 887–902. [CrossRef]
8. Okrugin, A.V.; Tolstov, A.V.; Sleptsov, A.P.; Baranov, L.N. Petrochemical Features of the Association of Ultrabasic Alkali Rocks and Carbonatites of the Tomtor Massif and Interpretation of Possible Trends of Their Evolution. *Arct. Subarct. Nat. Resour.* **2019**, *24*, 7–24. (In Russian) [CrossRef]
9. Vladykin, N.V.; Kotov, A.B.; Borisenko, A.S.; Yarmolyk, V.V.; Pokhilenko, N.P.; Salnikova, E.B.; Travin, A.V.; Yakovlev, S.Z. Age Boundaries of the Formation of the Tomtor Alkaline-Ultrabasic Massif: Results of Geochronological U-Pb and ^{40}Ar/^{39}Ar Studies. *Dokl. Earth Sci.* **2014**, *454*, 195–199. (In Russian) [CrossRef]
10. Skublov, S.G.; Tolstov, A.V.; Baranov, L.N.; Melnik, A.E.; Levashova, E.V. First Data on the Geochemistry and U-Pb Age of Zircons from the Kamaphorites of the Tomtor Alkaline-Ultrabasic Massif. Arctic Yakutia. *Geochemistry* **2020**, *80*, 125505. (In Russian) [CrossRef]
11. Lazareva, E.V.; Zhmodik, S.M.; Dobretsov, N.L.; Tolstov, A.V.; Shcherbov, B.L.; Karmanov, N.S.; Gerasimov, E.Y.; Bryanskaya, A.V. Major minerals of abnormally high-grade ores of the Tomtor deposit (Arctic Siberia). *Russ. Geol. Geophys.* **2015**, *56*, 844–873. [CrossRef]
12. Okrugin, A.V.; Zaitsev, A.I.; Borisenko, A.S.; Zemnukhov, A.L.; Ivanov, P.O. Gold-Platinum Placers of the Basin of the Anabar River and Their Possible Relationship with Alkaline-Ultrabasic Magmatites of the North of the Siberian Platform. *Otechestvennaya Geol.* **2012**, 11–21. (In Russian)
13. Okrugin, A.; Gerasimov, B. Paragenetic Association of Platinum and Gold Minerals in Placers of the Anabar River in the Northeast of the Siberian Platform. *Minerals* **2023**, *13*, 96. [CrossRef]

14. Okrugin, A.V.; Yakubovich, O.V.; Ernst, R.E.; Druzhinina, Z.Y. Platinum-bearing placers: Mineral associations and their ^{190}Pt-^{4}He and Re-Os ages, and potential links with large igneous provinces in the Siberian craton. *Econ. Geol.* **2020**, *115*, 1835–1853. [CrossRef]

15. Okrugin, A.V.; Zhuravlev, A.I. Mineralogical Criteria for Genetic Relationship of Igneous and Carbonatite Rocks of the Tomtor Massif (Siberian Platform). *IOP Conf. Ser. Earth Environ. Sci.* **2021**, *906*, 012104. [CrossRef]

16. Schairer, J.F.; Yoder, H.S. Crystal State and Melting of Simple Alkaline Basalts. In *Experimental Petrology and Mineralogy*; Makeev, V.I., Ed.; Nedra: Moscow, Russia, 1971; pp. 6–15. (In Russian)

17. Sheinmann, U.M. Ultrabasic-Alkaline Rocks Formation. In *Alkaline Intrusions. Their Location and Related Mineralization*; Gosgeoltehizdat: Moscow, Russia, 1961; pp. 15–54. (In Russian)

18. Milashev, V.A.; Krutoyarsky, M.A.; Rabkin, M.I.; Erlikh, E.N. *Kimberlites and Picrite Porphyry of North-Eastern Part of Siberian Platform*; Gosgeoltehizdat: Moscow, Russia, 1963. (In Russian)

19. Koval'sky, V.V.; Nikishov, K.N.; Egorov, O.S. *Kimberlites and Carbonatites of Anabar Anteclise*; Nauka: Moscow, Russia, 1969. (In Russian)

20. Egorov, L.S. *Melilites of Maymecha-Kotuy Province*; Nedra: Saint Petersburg, Russia, 1969. (In Russian)

21. Marshintsev, V.K. *Carbonatite Bodies of Eastern Slope of Anabar Uplift*; Kn. izd-vo: Yakutsk, Russia, 1974. (In Russian)

22. Frolov, A.A.; Lapin, A.V.; Tolstov, A.V.; Zinchuk, N.N.; Belov, S.V.; Burgomistrov, A.A. *Carbonatites and Kimberlites (Relationship. Minerageny. Prospecting)*; NIA-Priroda: Moscow, Russia, 2005. (In Russian)

23. Vladykin, N.V.; Torbeeva, T.S. Lamproites of Tomtor Massif (Eastern Preanabarie). *Geol. Geophys.* **2005**, *46*, 1038–1049. (In Russian)

24. Belov, S.V.; Lapin, A.V.; Tolstov, A.V.; Frolov, A.A. *Minerageny of Platform Magmatism (Trapps. Carbonatites. Kimberlites)*; SB RAS: Novosibirsk, Russia, 2008. (In Russian)

25. Holmes, A. A Contribution to the Petrology of the Kimberlite and Its Inclutions. *Geol. Soc. S. Afr.* **1936**, *39*, 379–428.

26. Zhuk-Pochekutov, K.A.; Gladkikh, V.S.; Leontiev, L.N. Association of Alkaline Basaltoids–Basalts of the Maymecha-Kotuy Volcanoplutonic Formation. In *Petrology and Geochemical Features of Complex Ultrasbasites and Carbonatites*; Nauka: Moscow, Russia, 1965; pp. 5–90. (In Russian)

27. Vasiliev, U.R.; Zolotukhin, V.V. *Petrology Af Ultrabasites of North of Siberian Platform and Their Some Genesis Issues*; Nauka: Novosibirsk, Russia, 1975. (In Russian)

28. Baranov, L.N.; Tolstov, A.V.; Okrugin, A.V.; Slepcov, A.P. New Data about Mineralogy and Geochemistry of Apatite-Magnetite Ores of the Tomtor Massif. North-East of the Siberian Platform. *Ores Met.* **2018**, *42–54*, 468. (In Russian) [CrossRef]

29. Vasiliev, U.R.; Kononenko, V.F.; Korolyuk, V.N. Accessory Chrome Spinels from Ultramafic Rocks of Maymecha-Kotuy Region. In *Genetic and Experimental Mineralogy Materials*; Nauka: Novosibirsk, Russia, 1976; pp. 7–16. (In Russian)

30. Genkin, A.D.; Distler, V.V.; Laputina, I.P. Chromite Mineralization of Differentiated Trapp Intrusions and It's Formation Parameters. In *Formation Conditions of Magmatic Ore Deposits*; Nauka: Moscow, Russia, 1979; pp. 105–126. (In Russian)

31. Chayka, I.F.; Zhitova, L.M.; Antsiferova, T.N.; Abersteiner, A.; Shevko, A.Y.; Izokh, A.E.; Tolstykh, N.D.; Gora, M.P.; Chubarov, V.M.; Kamenetsky, V.S. In-Situ Crystallization and Continuous Modification of Chromian Spinel in the "Sulfide-Poor Platinum-Group Metal Ores" of the Norilsk-1 Intrusion (Northern Siberia. Russia). *Minerals* **2020**, *10*, 498. [CrossRef]

32. Babushkina, S.A. Microcrystal Composition of Spinelids of Malokuonapskaya Pipe. *Otechestvennaya Geol.* **2008**, *906*, 85–95. (In Russian)

33. Sobolev, N.V.; Pokhilenko, N.P.; Lavrentiev, Y.G.; Usova, L.V. Composition Features of Chrome Spinels from Diamonds and Kimberlites of Yakutia. *Geol. Geophys.* **1975**, *16*, 7–24. (In Russian)

34. Afanasiev, V.P.; Zinchuk, N.N.; Pokhilenko, N.P. *Morphology and Morphogenesis of Indicator Minerals of Kimberlites*; GEO of SB RAS Publishing House: Novosibirsk, Russia, 2001. (In Russian)

35. Muan, A.; Huack, J.; Loffal, T. Equilibrium Studies with a Bearing on Lunar Rocks. In *Proceedings of the Third Lunar Science Conference*; Lunar and Planetary Science Institute: Houston, TX, USA, 1972; pp. 158–196.

36. Kushiro, I.; Schairer, J.F. New Data of Diopside-Forsterite-Silica System. In *Experimental Petrology and Mineralogy*; Nedra: Moscow, Russia, 1969; pp. 52–62.

37. Onuma, K.; Yagi, K. The System Diopside-Akermanite-Nepheline. *Am. Mineral.* **1967**, *52*, 227–243.

38. Schairer, J.F.; Yoder, H.S. The Nature of Residual Liquids from Crystallization. with Data on the System Nepheline-Diopside-Silica. *Am. J. Sci.* **1960**, *258-A*, 273–283.

39. Shkodzinsky, V.S. *Global Petrology According Modern Data of Hot Heterogenous Earth Accretion*; NEFU Publishing House: Yakutsk, Russia, 2018. (In Russian)

40. Wyllie, P.J. Problem of Formation Carbonatites in Relation with Experimental Data. Origin and Differentiation of Carbonatite Magma. In *Carbonatites*; MIR: Moscow, Russia, 1969; pp. 265–300.

41. Solovova, I.P.; Girnis, A.V.; Kogarko, L.N.; Kononova, N.N.; Stoppa, F.; Rosatelli, G. Composition of Magmas and Carbonate–Silicate Liquid Immiscibility in the Vulture Alkaline Igneous Complex. *Italy Lithos* **2005**, *85*, 113–128. (In Russian) [CrossRef]

42. Wyllie, P.J.; Lee, W.J. Kimberlites, Carbonatites, Peridotites and Silicate-Carbonate Liquid Immiscibility Explained in Parts of the System CaO-(Na$_2$O+K$_2$O)-(MgO+FeO)-(SiO$_2$+Al$_2$O$_3$)-CO$_2$. In Proceedings of the VIIth International Kimberlite Conference, Cape Town, South Africa, 11–17 April 1998; pp. 923–932.

43. Kapustin, Y.L. Differentiated Sill of Basaltoids and Excretion Features in It of Calcite. *Zapiski VMO* **1985**, 275–288. (In Russian)

44. Panina, L.I.; Motorina, I.V. Liquid Immiscibility of Deep Magmas and Nucleation of Carbonatite Melts. *Geochemistry* **2008**, *46*, 487–504. (In Russian)
45. Delicin, L.M.; Melentiev, G.B.; Batenin, V.M.; Tolstov, A.V. The Coexistence of Two Immiscible Liquid Phases in Silicate-Salt Niobium-Rare Earth System. *Dokl. RAS* **2014**, *462*, 440–443. (In Russian)
46. Ernst, R.E.; Hamilton, M.A.; Söderlund, U.; Hanes, J.A.; Gladkochub, D.P.; Okrugin, A.V.; Kolotilina, T.; Mekhonoshin, A.S.; Bleeker, W.; LeCheminant, A.N.; et al. Long-Lived Connection between Southern Siberia and Northern Laurentia in the Proterozoic. *Nat. Geosci.* **2016**, *9*, 464–469. [CrossRef]